J. A. Bucholz, "Physics Analyses in the Design of the HFIR Cold Neutron Source," pp 29-40, BgNS Transactions, Vol 5, No. 1, July 2000, which was a special issue dedicated to the "XIII International School on Nuclear Physics, Neutron Physics, and Nuclear Energy" held in Varna (Bulgaria), Sept 27-Oct 3, 1999

* BgNS = Bulgarian Nuclear Society

PHYSICS ANALYSES IN THE DESIGN OF THE HFIR COLD NEUTRON SOURCE

James A. Bucholz

Oak Ridge National Laboratory, Oak Ridge, Tennessee 37831, USA

Physics analyses have been performed to characterize the performance of the cold neutron source to be installed in the High Flux Isotope Reactor[1] at the Oak Ridge National Laboratory in the near future. This paper provides a description of the physics models developed, and the resulting analyses that have been performed to support the design of the cold source. These analyses have provided important parametric performance information, such as cold neutron brightness down the beam tube and the various component heat loads, that have been used to develop the reference cold source concept.[2,3]

1. Facility/Model Description, Physics Codes, and Cross-Section Data Sets

1.1. HFIR Description

The High Flux Isotope Reactor[1] at ORNL is a multifunction research reactor that has facilities for isotope production, materials irradiation, and neutron beam experiments. It consists of a water-cooled annular core in a beryllium reflector. Several key physics parameters associated with the core are shown in Table 1. A number of positions in the central hole are used primarily for isotope production. Outside the fueled core region, the removable portion of the beryllium reflector has 12 (RB) irradiation positions and 8 control rod access plugs, while the permanent reflector has 22 vertical experiment facilities (VXF positions), a pneumatic tube, a slanted engineering facility, and four horizontal beam tubes that are used for neutron scattering experiments. Originally designed to operate at 100 MW, the reactor has been operating at only 85 MW since 1987, but restoration to 100 MW operation will be considered after a series of upgrades which are to begin in FY 2000. The feasibility of retrofitting one of the beam tubes with a liquid hydrogen cold source for neutron scattering experiments was first studied in 1995, and has since moved through the pre-conceptual design phase[2], the conceptual design phase[3] (reported here), and the final detailed design phase. The HB-4 horizontal beam tube was selected as the preferred location for the new cold source because the tangential orientation of the tube relative to the core would minimize the fast neutrons and hard gammas streaming down the beam tube, and because the orientation of this particular beam tube permitted the construction of a cold source guide hall adjacent to the reactor building. In addition, the thermal flux at this location was determined to be higher than at the Institut Laue-Langevin (ILL) vertical cold source location[4].

The cold source physics analyses are, of course, greatly dependent on the model used to represent the HFIR reactor, which is the source of neutrons reaching the cold source. The 3-D reactor core model used in these studies is believed to be the most detailed physics model of the HFIR that has been developed. This model has been and will continue to be reviewed by HFIR staff to ensure an accurate representation of the HFIR system. Validation of the reactor model has been performed by comparisons with measured data. It should be noted that although at present the HFIR operates at 85 MW, all calculations were based on 100 MW, in anticipation of the potential return to this power level.

Figure 1 shows a cross-section of the HFIR core and reflector at the reactor's midplane, as modeled in the current 3-D Monte Carlo analyses, while Fig. 2 shows an isometric view of the cold source capsule and two different cross sectional views of it as modeled in the current 3-D Monte Carlo analyses. The supercritical liquid hydrogen flowing through the capsule at 20 °K would fill the region between the thin hemispherical aluminum shell on the outside of the

capsule and the thin ellipsoidal shell on the inside. The capsule has an outer diameter of 9.84 cm, while the moderator region between the two shells is approximately 5.0 cm thick. As shown in Fig. 1, the cold source capsule will reside inside a thin-walled aluminum vacuum vessel which will be placed inside the tip of the HB-4 beam tube, adjacent to the beryllium block between the HB-1 and HB-4 beam tubes. It should also be noted that two thin aluminum windows further down the beam tube, in the cold neutron beam path, have been incorporated into the design and are included in the analytic model.

Table 1. Key HFIR physics parameters.[1]

Parameter	Value
Power level	100 MW
Maximum fuel cycle length	23 days
Active fuel height	50.80 cm
Active fuel region volume	50.69 L
U^{235} loading	9.4 kg
Total B^{10} burnable poison loading	2.8 g
Fuel plate thickness	0.1270 cm
Cladding thickness	0.0254 cm
Coolant channel thickness	0.1270 cm

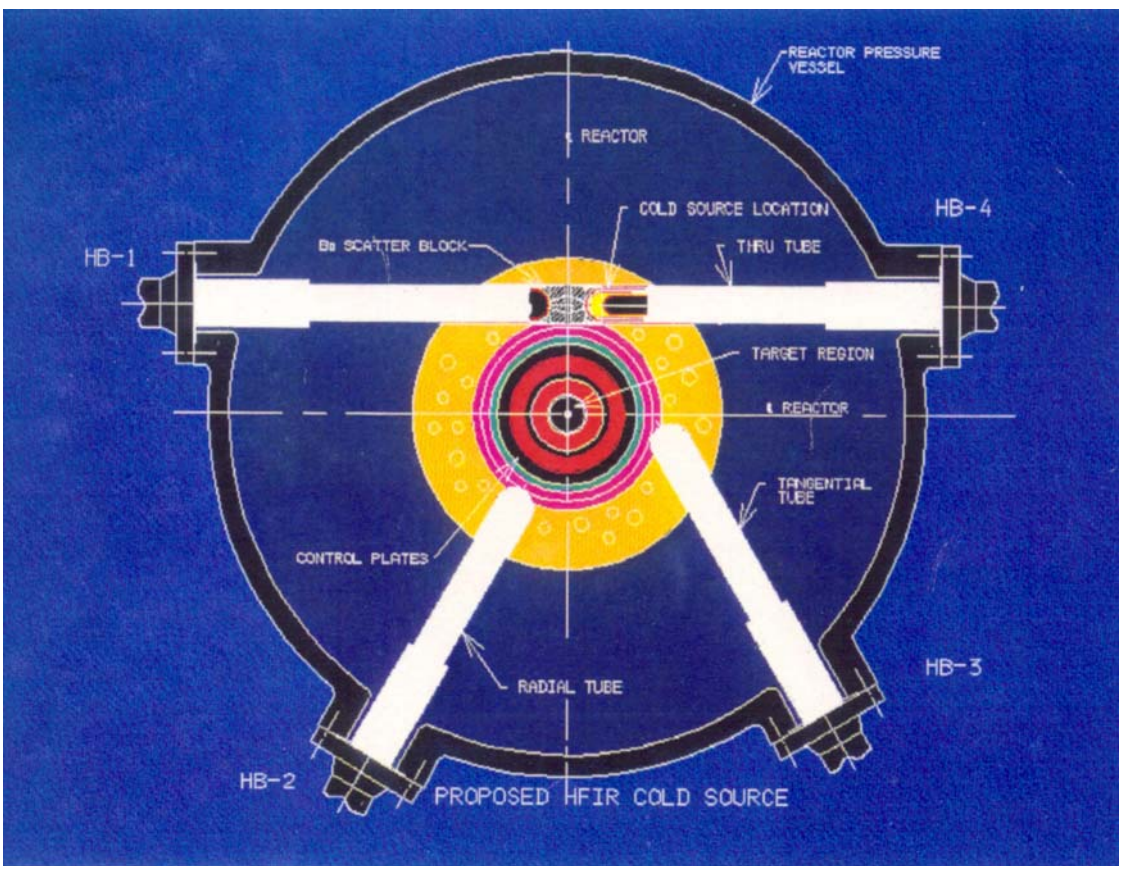

Fig. 1. HFIR reactor core midplane layout.

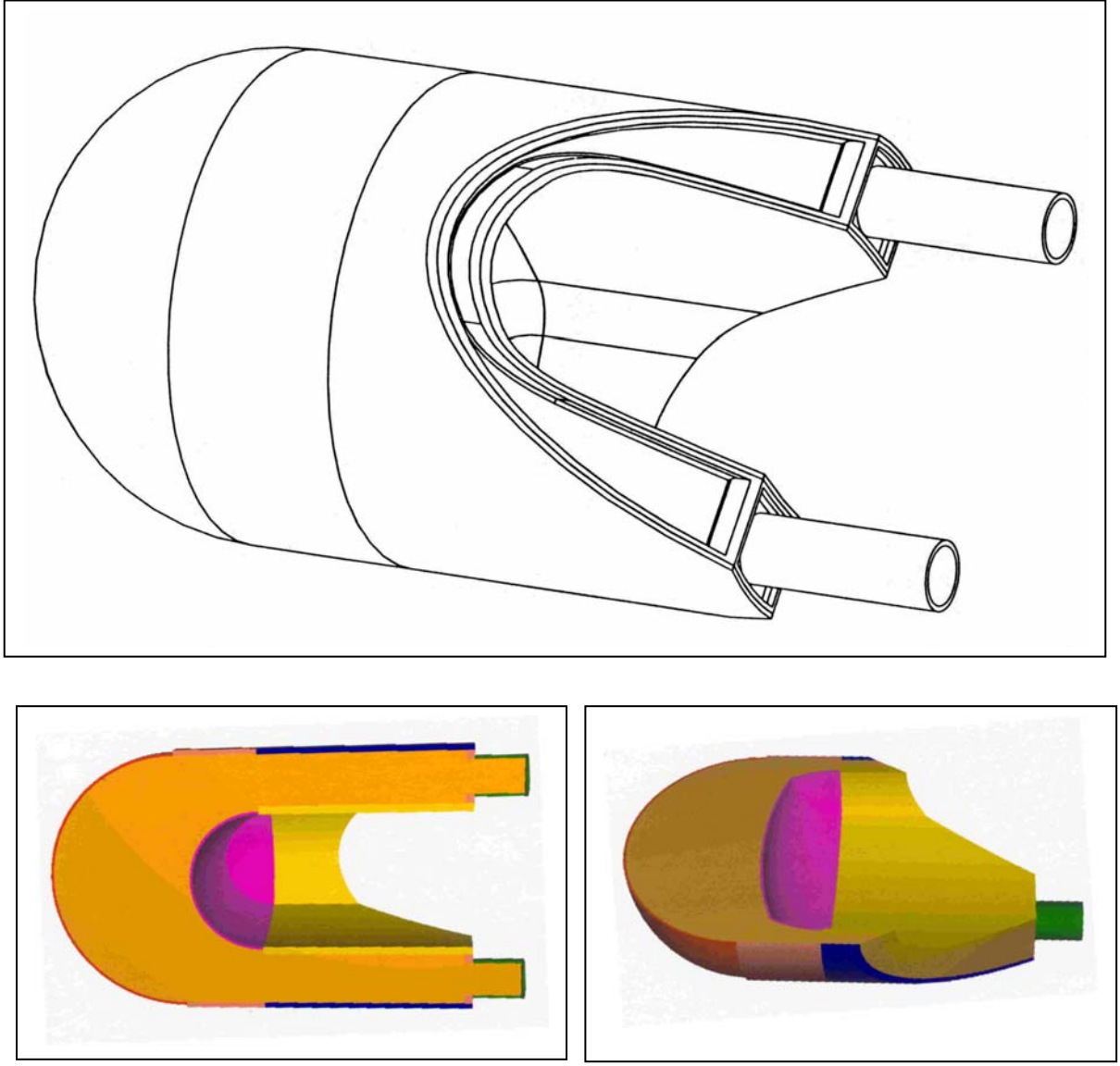

Fig. 2. Cold source capsule as modeled in MCNP, including horizontal and vertical slices.

1.2. Codes and Cross-Section Data

Because of the inherent 3-D nature of the HFIR core, the various experimental and user facilities in the reflector, and the location of the proposed cold source in the HB-4 beam tube, the 3-D MCNP Monte Carlo code[5] (Version 4b) was used in virtually all of the analyses performed to date. In addition to being able to model all aspects of the 3-D geometry, it also has the advantage of being able to represent all of the cross-section data on a pointwise energy basis. Various pointwise cross-section libraries are typically supplied with the MCNP code. Each is the result of different historical evaluations of the cross-section data for the various nuclides. Except for U-235, Al-27, para hydrogen, and ortho hydrogen, the data used here corresponds to the Los Alamos National Laboratory (LANL) recommended data set for each nuclide. In the case of the U-235, the recommended data set from LANL was modified so as to include the energy-dependent delayed fission product gammas as regular secondary gammas. (Normally delayed fission product gammas are not included in the regular MCNP gamma production cross sections, and one needs to determine these sources off-line with ORIGEN[6] and then run a second MCNP calculation with only these source terms present.) By now treating them as regular secondary gammas, one can track those gammas without approximation (just like the prompt gammas)

and determine where in the system that energy is deposited without the persistent need for a second MCNP calculation. In the case of Al-27, the recommended data set from LANL was modified so as to include, as regular secondary gammas, those decay gammas coming from the short-lived Al-28 produced by thermal neutron capture in Al-27. By accounting for these gammas in this fashion, we can automatically track those gammas without any approximations and determine where that energy is deposited rather than where it is first created. In the case of the para hydrogen and ortho hydrogen in LH_2 at 20 °K (0.0726 g/cc), it was determined that the new (as yet unreleased) LANL evaluation of the Institut Fur Kernenergetik Und Energiesysteme (IKE) data from Germany[7] was superior to previous data files based on measurements and analyses performed at the National Institute of Standards and Technology (NIST).

Using the most detailed physics model of the HFIR that has been developed (with no artificial adjustments), 3-D MCNP calculations routinely yield a k_{eff} between 1.006 and 1.008 (±0.0006) for all cases of interest: at beginning-of-cycle (BOC), middle-of-cycle (MOC), and end-of-cycle (EOC) when the depleted fuel compositions and known control rod positions are used in the MCNP model. In these cases, depleted fuel compositions for each of 17 radial zones and 7 axial zones are explicitly represented in the MCNP models. Compositions during the lifetime of the core were obtained using 3-D VENTURE depletion analyses[8] with control-rod-follow capability.

1.3. Source Terms Used in the Analyses

Neutron-only k_{eff} calculations were used to determine the neutron source distribution in the core. The core model used in most analyses assumed EOC fuel concentrations. This was done in order to obtain a realistic upper limit on the cryogenic heat loads that peak at EOC.

Acceptable statistical uncertainties (less than 2-3%) at the various point detectors of interest generally required 288 batches of 10,000 source neutrons, for a total of 2,880,000 histories, although the results from the first 20 batches (300,000 histories) were typically discarded as the source distribution within the core was being converged. Final reference results were performed with 1224 batches of 10,000 source neutrons, for a total of 12.24 million histories. Reportable results were, therefore, based on the remaining histories after the source was deemed converged. These calculations were typically performed on the IBM SP-2 multinode cluster of workstations.

1.4. Method Used for Calculating the Brightness

The cold neutron beam magnitude is typically expressed in terms of its "brightness," which is defined as the "number of neutrons per second, per square centimeter, per angstrom, per steradian" at a point detector 477.7 cm from the center of the former HB-1/HB-4 through tube, or 466.1 cm from the cold source capsule. Throughout this study, the calculated brightness is tabulated in seven energy bands as defined in Table 2. These energy bands provide data over the range of interest as defined by the proposed cold source instruments presented in Table 3.

To determine the brightness of the neutron beam down along the HB-4 beam tube, a point detector estimate of the energy-dependent scalar flux was tabulated at the above location, along the centerline of the HB-4 beam tube. More specifically, the model only tabulated a select portion of the scalar flux at that point detector. Looking back from that point, the liquid hydrogen cold source (having a diameter of 9.843 cm) would subtend an angle of ±0.60 degrees about the beam tube centerline, or a solid angle of 3.5×10^{-4} steradians. To ensure that the MCNP tally counter associated with that point detector counted only neutrons traveling within that solid angle, next event estimates of the flux at that point were made only from collision sites in the cold source and those material regions directly behind the cold source. Specifically, this included only the

following regions: the liquid hydrogen and aluminum forming cold source capsule, and those portions of the vacuum vessel, beam tube, water space, and beryllium block further back, that are directly behind a 9.843-cm-diam disk corresponding to the diameter of the cold source capsule. Next event flux estimates from all other collision sites were ignored by setting the probability of a contribution from these other cells to zero. This not only had the desired effect of selectively tallying only those neutrons traveling within the desired range of solid angular directions, but it also allowed the calculations to proceed about five times faster than they would have if next event flux estimates were made from all collision sites in the problem.

Table 2. Energy bands of interest.

Corresponding neutron energy range (eV)	Wavelength range (angstroms)
0.01000-0.10400	0.89-2.86
0.00325-0.01000	2.86-5.02
0.00145-0.00325	5.02-7.51
0.00085-0.00145	7.51-9.81
0.00058-0.00085	9.81-11.93
0.00033-0.00058	11.93-15.86
0.00010-0.00033	15.86-28.60

Table 3. Proposed cold source instruments.

Instrument type	Wavelength (angstroms)
SANS 1 (D11)	7 - 15
SANS 2	6
SANS 3 (short ORNL)	4.7
Triple-axis	1.8 - 6
Reflectometer	5
Biology single-crystal (DB 21)	8
Cold neutron test station	6 – 30

1.5. Methods Used for Calculating Neutron and Gamma Heating

Estimates of the neutron and gamma heating in the liquid hydrogen and in the various aluminum components around the cold source were originally obtained by two independent methods. Both methods rely on region-averaged estimates of the total neutron or gamma track length in the various cells comprising the system. In the first method, the average energy-dependent neutron or photon heating number (MeV/collision) available in the MCNP cross-section libraries is folded with the total (pointwise energy-dependent) neutron or gamma cross-section, which is then folded with the (pointwise energy-dependent) neutron or gamma track length estimates of the flux each time a neutron or photon passes through a cell of interest. These values are then integrated over all energy and spatially averaged over the volume of the respective cells to obtain the specific neutron and gamma heating rates in terms of watts/gram. In the second method, the cell-averaged neutron and gamma fluxes in the aluminum-filled cells were first tallied in multigroup energy bins corresponding to the 39n/44g group structures used in the analysis of the Advanced Neutron Source (ANS) reactor.[9] These multigroup neutron and gamma fluxes were then folded with the multigroup neutron and gamma kerma factors described in Appendix D of Ref. 9 to obtain the average specific heating rate (watts/gram) for the various cells. (These multigroup kerma factors were based on the KAOS-V kerma factor data library[10] available from Argonne National Laboratory (ANL) and/or the Radiation Safety Information Computational Center in Oak Ridge.) After several such calculations showed the directly-calculated MCNP heating rates to be in good agreement with those calculated indirectly using the multigroup data, the latter procedure was dropped.

Lastly, nuclear heating in the aluminum due directly or indirectly to neutron radiation has three separate components: that produced directly because of the kinetic interactions between the neutrons and the aluminum, that produced because of the subsequent gamma decay of Al-28 atoms that become activated by thermal neutron absorption in the Al-27, and that produced because of the subsequent beta decay of Al-28 atoms that become activated by thermal neutron absorption in the Al-27. The cell-averaged neutron heating rate tallies used here for cells containing aluminum account for all three processes. Basically, the pointwise energy-dependent flux is folded with the pointwise total cross-section and the energy-dependent neutron heating number (MeV/collision) to obtain the direct component. In addition, the pointwise flux is also folded with the pointwise Al-27 absorption cross-section to obtain the Al-28 production rate, which is then folded with the average beta decay energy (1.2423 MeV). This approach is based on the assumption that the Al-28 decay beta deposits its energy at the point where it is created. The Al-28 decay gammas, on the other hand, do not generally deposit their energy where they are created. Using the newly modified Al-27 cross sections described above, these Al-28 decay gammas are now treated as additional secondary gammas (produced by neutrons interacting with Al-27). With this scheme, these gammas are then tracked by MCNP (along with all other secondary gammas), depositing their energy in various components along the way. This approach inherently models all points of origin exactly, and tracks the gammas until all of the energy has been deposited in various structures. The only minor disadvantage is that, in a given component, these contributions are now indistinguishable from all other secondary gammas. Still, the added convenience and improved accuracy of this approach far outweigh this one small disadvantage.

2. Brightness, Gain Factors, and Comparisons with Existing Facilities

Table 4 shows the brightness of the 5-cm-thick HFIR cold source in the seven energy bands of interest, as well as the comparable values for the horizontal cold source in the ILL reactor. These comparisons suggest that the proposed HFIR cold source will be comparable to the ILL cold source.

Although a full validation of the HFIR calculations has not yet been undertaken, some evaluations were performed to determine if they were consistent with existing data.
Two questions were addressed:

1. Are the calculated thermal neutron fluxes at the cold source location (without the cold source in place) consistent with expected values?

2. Are the gains in longer wave neutron fluxes consistent with gains measured at existing hydrogen cold source facilities?

The first question addresses the ability of the model to calculate the physics of the reactor core and to transport the neutrons to the cold source location. In order to answer this question, a comparison was made with previously reported HFIR fluxes. Although comparisons with identical geometry could not be made, the fluxes were roughly comparable, and the differences can in general be explained by the geometry differences. The gain factor issue was addressed by comparing the calculated gain factors associated with the HFIR cold source (as shown in Table 5) with gain factors measured at other hydrogen cold source facilities as reported in Ref. 4. This comparison is summarized by Fig. 3, where the calculated gain factors for the HFIR hydrogen cold source are plotted as a function of neutron wavelength along with reported values from existing hydrogen cold source facilities. There, the gain factors for the HFIR cold source can be seen to be very consistent with those at other facilities.

Table 4. Neutron brightness comparison between the HFIR cold source and the ILL horizontal cold source

Wavelength (angstroms)	Neutron energy range (meV)	HFIR cold source brightness[a] ($s^{-1}cm^{-2}A^{-1}sr^{-1}$)	ILL horizontal cold source brightness[b] ($s^{-1}cm^{-2}A^{-1}sr^{-1}$)	Ratio HFIR/ILL
0.887-2.86	10.00-104.0	1.09×10^{13}	7.72×10^{12}	1.41
2.86-5.02	3.25-10.0	7.54×10^{12}	4.05×10^{12}	1.86
5.02-7.51	1.45-3.25	1.55×10^{12}	1.39×10^{12}	1.12
7.51-9.81	0.85-1.45	3.99×10^{11}	4.00×10^{11}	1.00
9.81-11.93	0.58-0.85	1.56×10^{11}	1.49×10^{11}	1.05
11.93-15.86	0.33-0.58	5.44×10^{10}	5.64×10^{10}	0.96
15.86-28.60	0.10-0.33	7.54×10^{9}	Not available	---

[a] HFIR data based on MCNP calculations at 100 MW with statistical standard deviations below 2% with the exception of the lowest energy group where the statistical standard deviation is 2.6%.

[b] Average values over energy range as estimated from Fig. 5 of a paper presented by Ageron[4] at the 1990 International Workshop on Cold Neutron Sources.

Table 5. Gain factors as calculated for the proposed HFIR liquid hydrogen cold source

Wavelength (angstroms)	Neutron energy range (meV)	HFIR brightness with LH2 cold source ($s^{-1}cm^{-2}A^{-1}sr^{-1}$)	HFIR brightness without LH2 cold source ($s^{-1}cm^{-2}A^{-1}sr^{-1}$)	Gain ratio
0.887-2.86	10.0-104.0	1.09×10^{13}	3.79×10^{13}	0.29
2.86-5.02	3.25-10.0	7.54×10^{12}	1.61×10^{12}	4.68
5.02-7.51	1.45-3.25	1.55×10^{12}	1.16×10^{11}	13.36
7.51-9.81	0.85-1.45	3.99×10^{11}	1.95×10^{10}	20.46
9.81-11.93	0.58-0.85	1.56×10^{11}	Not available	---
11.93-15.86	0.33-0.85	5.44×10^{10}	Not available	---
15.86-28.60	0.10-0.33	7.54×10^{9}	Not available	---

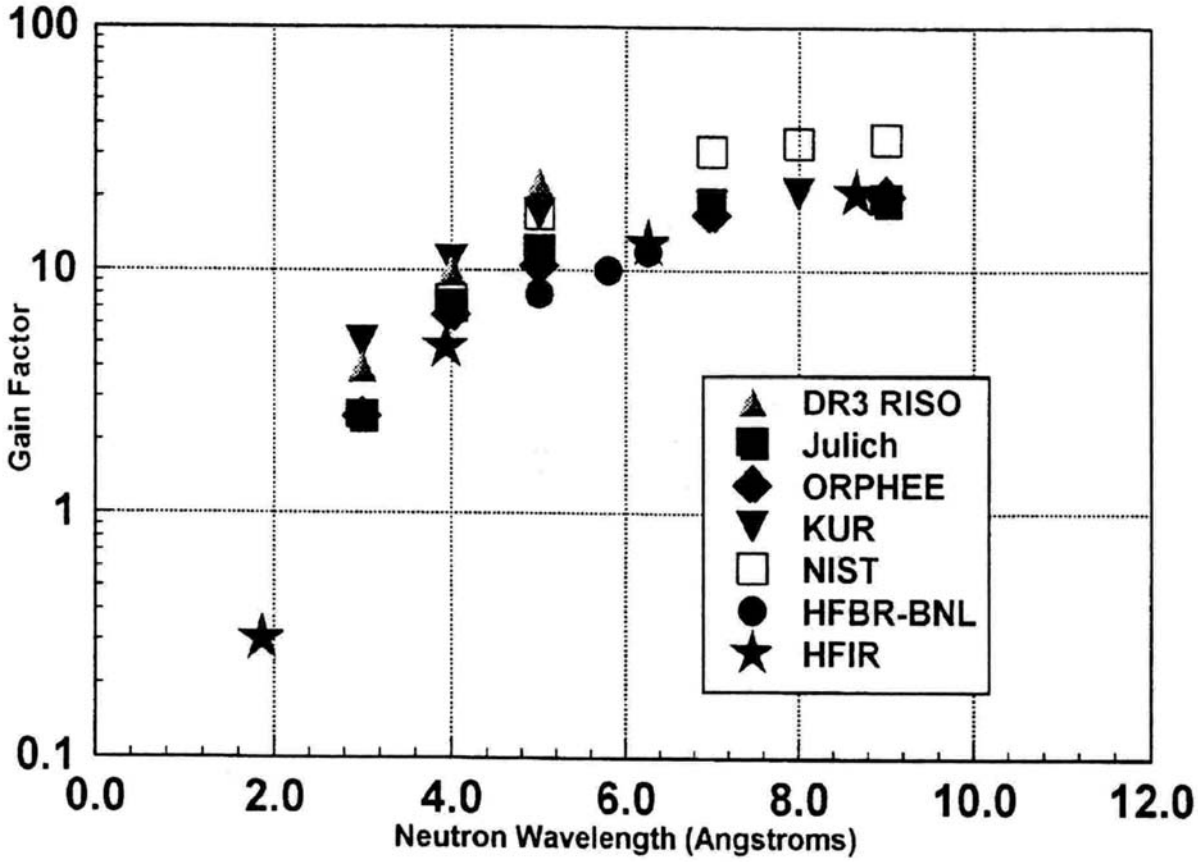

Fig. 3. Calculated HFIR gain factors compared with other facility gain factors.

3. Nominal Heat Load Calculations

Accurate determination of the overall heat load associated with the cold source is quite important since this will define the cooling requirements for the cryogenic cooling system. Especially important are the heat loads associated with the liquid hydrogen, the aluminum capsule containing the liquid hydrogen, and the inlet and outlet tubes carrying the liquid to and from the cold source. In addition, one must also consider the intrinsic heat load associated with pumping the liquid hydrogen through the system. This aggregate heat load must all be removed by the cryogenic cooling system. In addition, there is concern with the heat load associated with the cold source vacuum vessel, which is a separate component between the cold source capsule and the inner wall of the beam tube. Even though this heat load will not have to be removed cryogenically, the design must still supply adequate cooling.

To estimate the total nuclear heat load in the cold source and other components, one must consider energy deposited by prompt fission gammas from the core, delayed fission gammas from the core, and secondary gammas produced in all components, as well as energy deposited directly by neutrons from the core, and the energy deposited by the decay gammas and decay betas from the disintegration of the short-lived Al-28 that is constantly being produced by neutron activation of Al-27. For the cold source, non-nuclear intrinsic heat loads such as frictional heating and conventional thermal radiation must also be considered, although the latter can be shown to be negligible. Once these specific heat loads (watts/g) were determined using the standard neutronic model, the volumes and masses of the corresponding cells in the design were used to estimate the

actual heat loads. Table 6 shows the origin and distribution of the nominal cryogenic heat loads (in watts) associated with the cold source when the HFIR is operating at a power of 100 MW. As indicated in this table, the total cryogenic heat load was estimated to be approximately 2.2 kW.

The uncertainty to be applied to the nominal heat load calculation is a separate issue. In the past, large uncertainty factors (40% and higher) have been applied to the calculated heat loads. It is believed that today the calculational techniques and models are better than this and, thus, that it represents an overly conservative approach that translates to additional costs. Therefore, a heat load measurement will be conducted in HFIR close to the proposed cold source location and used to develop a defendable uncertainty factor. A 40% uncertainty factor, however, was used to define the refrigerator requirement, which was a long-lead procurement item. This did not add substantially to the cost of the refrigerator and should give us additional margin if the efficiency of the refrigerator performance declines with age.

Table 6. Nominal cryogenic heat loads for the reference HFIR cold source

Source of heating	Liquid hydrogen (W)	Aluminum structure (W)	Total (W)	Percent of system total
Gamma (primary, secondary, delayed fission, Al-28 decay)	244.8	1025.2	1270.0	57.4
Direct neutron heating	316.7	8.9	325.6	14.7
Beta decay of short-lived Al-28	0.0	227.8	227.8	10.3
Nuclear heating of inlet/outlet tubes[a]	31.5	157.6	189.1	8.6
Total nuclear heating	593.0	1419.5	2012.5	91.0
Intrinsic system heating			200.0	9.0
Total cryogenic heat load			2212.5	100.0

[a] Value is based on a 0.9525-cm inside diameter (ID) inlet tube and a 1.27-cm-ID outlet tube, both with a 0.0991-cm-thick aluminum wall.

4. Design Optimization Studies

A number of physics studies have been performed in arriving at the present reference design concept. Several of the studies reported in this section were documented in the pre-conceptual design report[2] and are included here for completeness while the early hydrogen thickness sensitivity studies have been significantly supplemented and revised as noted in Sect. 4.1.

4.1. Impact of Variations in the Ortho/Para Hydrogen Ratio in the LH_2

A parametric evaluation was first performed to determine the sensitivity of the cold source performance to the ortho/para hydrogen ratio.

In liquid hydrogen (H_2), the spin states of the two protons may be aligned in parallel as in ortho hydrogen, or anti-parallel as in para hydrogen. Left undisturbed at cryogenic temperatures for many hours, the two protons forming H_2 will seek the lowest energy state, and para hydrogen will become the predominant form, although neutron irradiation can and does cause the hydrogen to transition back to the ortho state. Figure 4 shows that for neutrons below about 0.03 eV (30 meV), the total neutron scattering cross sections for ortho-H and para-H are very different, with that for ortho-H being more than an order of magnitude higher than that for para-H. This affects the slowing down probability and the total number of collisions in a cold source of finite size. As a practical matter, it is difficult to know or to measure the amount of either species present at any time.

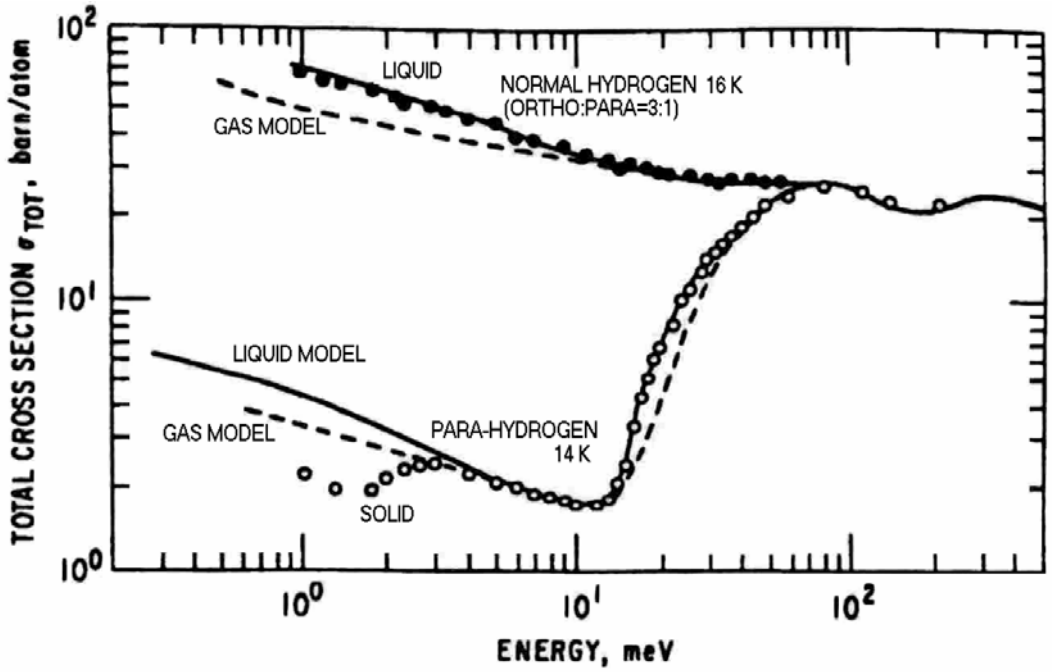

Fig. 4. Total scattering cross sections for normal hydrogen (ortho:para=3:1) and for para hydrogen. (Taken from Fig. 12 of Ref. 11.)

Previous analyses[2] had indicated that the ortho/para hydrogen ratio had little impact on the optimal hydrogen thickness for the proposed geometric shape of the HFIR cold source. This was found to be inconsistent with evaluations performed at NIST, and, therefore, a decision was made to create a simplified model of the NIST cold source geometry and examine the spectrum changes when the ortho/para ratio was significantly changed. The results are illustrated in Fig. 5. As seen from this figure, the 65% ortho case and the all-para case have significantly different spectral shapes in the 1-8 meV region. This was comforting insofar as the spectral shapes for these two cases were found to be very consistent with those previously reported by NIST[12]. Still, the results were also perplexing since the spectral shapes were very different from those previously calculated for the HFIR cold source (cf. Fig. 6).

To resolve this and gain a better physical understanding of the differences between the two systems, the simplified NIST cold source geometry model was slowly and methodically modified in ten incremental steps until it resembled the HFIR cold source geometry. Using MCNP, spectral calculations were performed for each of the intermediate geometries in this "evolution study." The ten configurations studied are shown in Fig. 7. The simplified NIST geometry, represented by configuration A, consists of a large, hollow, 2-cm-thick spherical shell of LH_2

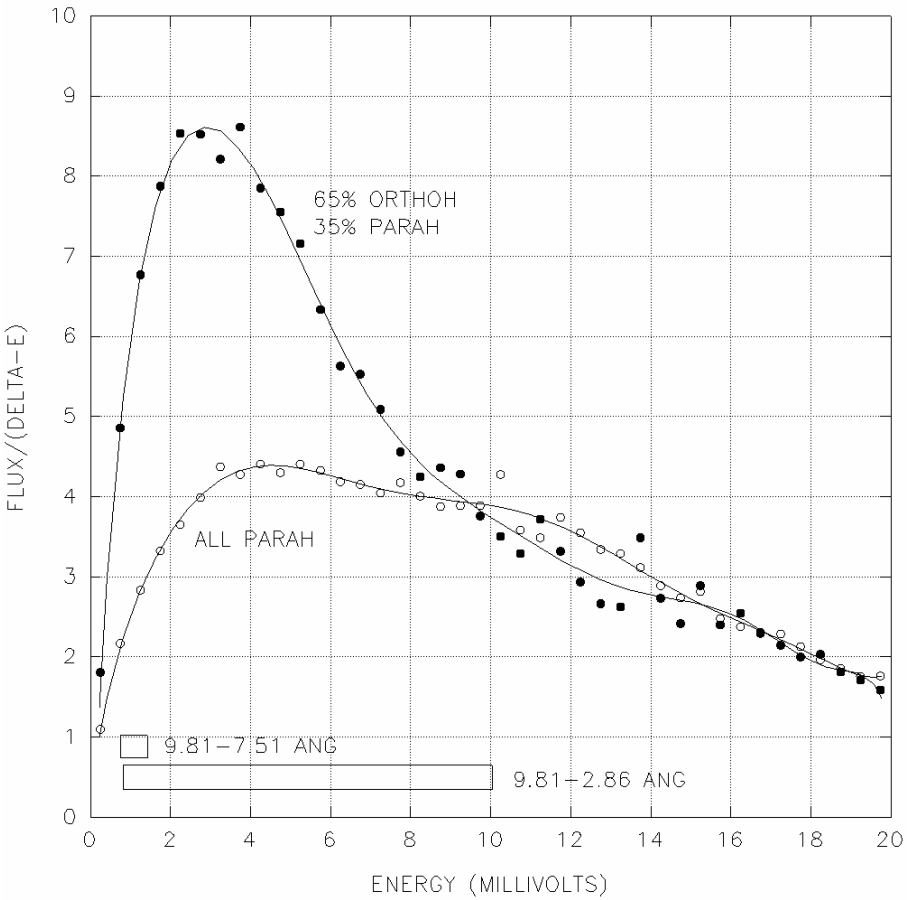

Fig. 5. Ortho hydrogen impact on flux spectrum in NIST cold source geometry. This corresponds to a 32-cm-diam x 2-cm-thick "punctured" spherical shell of LH_2 in a heavy water reflector, like the idealized NIST geometry shown in Fig. 7(A), with the flux calculated at a point 940.9 cm down a 20-cm-diam beam tube corresponding to an angle of ±0.60 degrees.

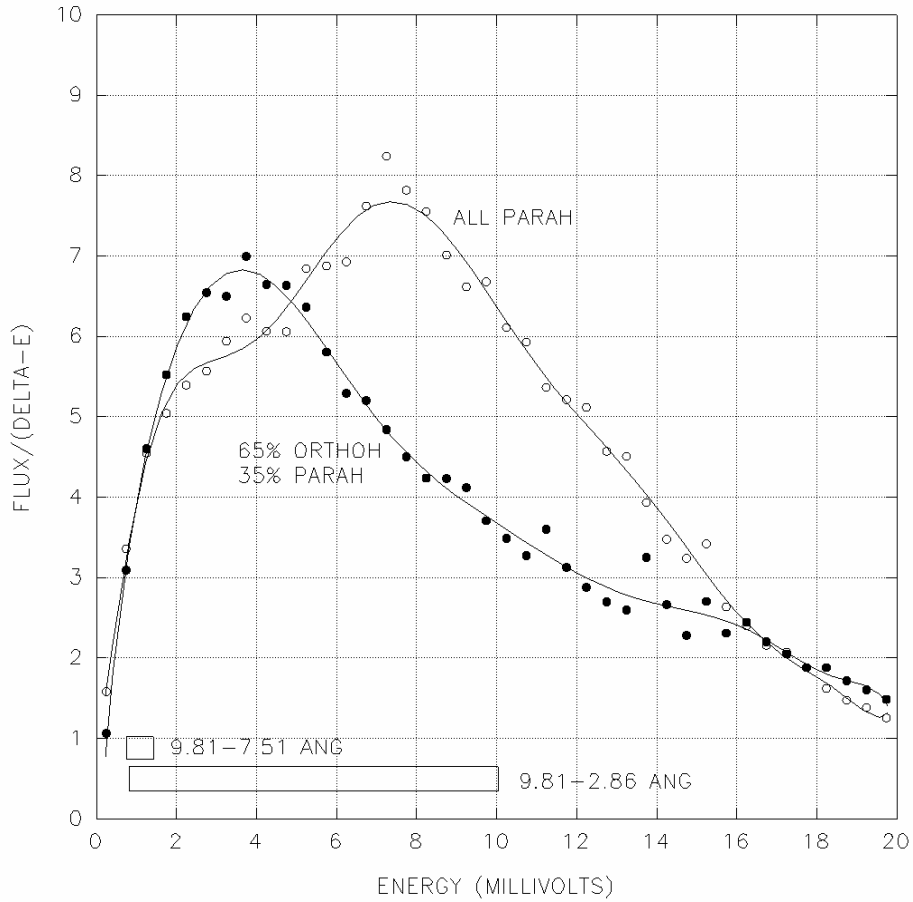

Fig. 6. Ortho hydrogen impact on flux spectrum in HFIR cold source geometry. This corresponds to a 10-cm-diam "dented" sphere of LH_2 (with coolant tubes and transition region) in a beryllium reflector, like the idealized HFIR geometry shown in Fig. 7(J), with the flux calculated at a point 477.7 cm down a 10-cm-diam beam tube, corresponding to an angle of ±0.60 degrees.

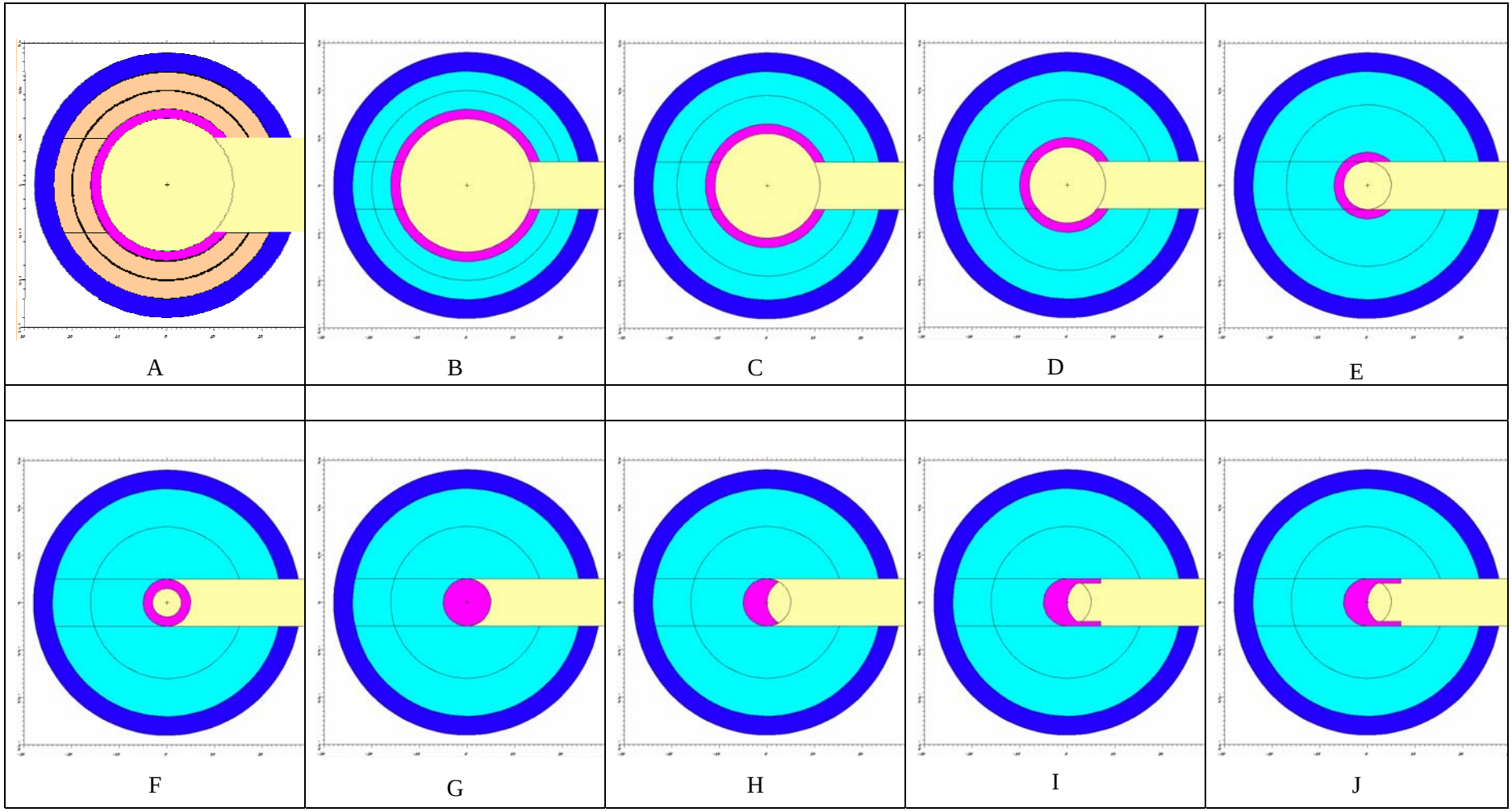

Fig. 7. Series of different cold source geometry configurations used in "the evolution study." The purpose of these calculations was to study "qualitatively" how the physics changes, and how the resulting flux spectra (with and without ortho-H) change, as one moves slowly and methodically from a NIST-like cold source configuration to a HFIR-like configuration using a series of idealized academic models.

with an outside diameter of 32 cm. It is surrounded by a heavy water reflector. The dark outermost region in this configuration, beyond the buffer region representing the reflector, contains a 300 °K Maxwellian source of thermal neutrons. This same source was used in all ten configurations studied so that the results obtained would be directly comparable in all cases. Spectral results for configuration A of Fig. 7, with and without ortho-H, are shown in Fig. 5.

In configuration B, the diameter of the beam tube was reduced from 20 cm to 10 cm, and the heavy water reflector was replaced with a beryllium reflector containing trace amounts of ^{3}He and equilibrium ^{6}Li (as known to exist in the HFIR reflector). In this case, the inner spherical shell of LH_2 was left unchanged (OD=32 cm). In configurations C, D, and E, the outer diameter of the LH_2 moderator shell was reduced to 26 cm, 20 cm, and 14 cm. Qualitatively, the spectral shapes for configurations B through D were all very similar to those for configuration E, shown in Fig. 8. (A full set of spectral plots may be found in Appendix A of Ref. 3.) In all these configurations, the spectrum for the all-para case exhibits a low-energy plateau and, in all these cases, the 65% ortho case would serve as a much better cold source. This low-energy plateau for the “all-para” cases with the beryllium reflector is due to the fact that the thin, high-leakage, all-para cold source is not producing many cold neutrons and the fact that the beryllium reflector (with trace amounts of thermal neutron absorbers) is absorbing most of those that are produced. In the NIST-like configuration with the heavy water reflector, this absorption in the reflector is not significant and only a small fraction of the cold neutrons produced are absorbed.

As one goes from the "punctured" 14-cm-diam x 2-cm-thick spherical shell in configuration E of Fig. 7 to the "complete" 10-cm-diam x 2-cm-thick spherical shell in configuration F, the basic physics changes markedly and the resulting spectral shapes for the all-para case are notably different for good physical reasons. (Spectral shapes for these two configurations may be seen in Figs. 8 and 9 respectively.) The "punctured sphere" in configuration E is still a thin, high-leakage system where the small amount of slowing-down afforded by scattering in the para hydrogen cannot keep up with the absorption in the reflector and the leakage down the beam tube. The all-para system is simply undermoderated and there is insufficient opportunity for neutrons to scatter down to lower energies before escaping down the beam tube. Indeed, the backside of the LH_2 moderator is only 2 cm thick. (That is why the addition of ortho-H with its higher scattering cross section can so dramatically improve the performance in this case.) In configuration F, however, one now has a "complete" spherical shell of LH_2. Neutrons scattering from the backside of the spherical shell still have the opportunity to scatter in the LH_2 on the frontside of the shell before escaping down the beam tube. More importantly, the higher-energy neutrons that would have escaped down the beam tube, now have an opportunity to interact with LH_2 in the frontside and get scattered back to other portions of the LH_2 sphere, where they may now slow-down further. This makes the LH_2 much more effective -- so much so that even the para-H with its relatively small scattering cross section can now provide a near-optimal degree of moderation, so that any further scattering contributions by the ortho-H are almost inconsequential (see Fig. 9). Indeed, once the geometry is such that the all-para case can provide near-optimal moderation, any substantial amount of ortho-H (or any additional thickness of para-H) may prove deleterious to the cold neutron spectrum insofar as any additional scattering events (beyond the optimal number) will serve only to increase the retention time, the total number of collisions, and hence the probability of absorption by the hydrogen itself. This latter effect is clearly visible in the spectral shapes for the solid sphere in configuration G (not shown here due to space limitations) where the 65% ortho case produces 20-30% fewer cold neutrons in the 7.5 to 9.8 angstrom range than the all-para case. Still, the spectral shapes for configurations G through J are all very similar to those shown in Fig. 9 for configuration F. For completeness, the spectral shapes for the idealized model of the HFIR cold source (configuration J) are shown in Fig. 6 above.

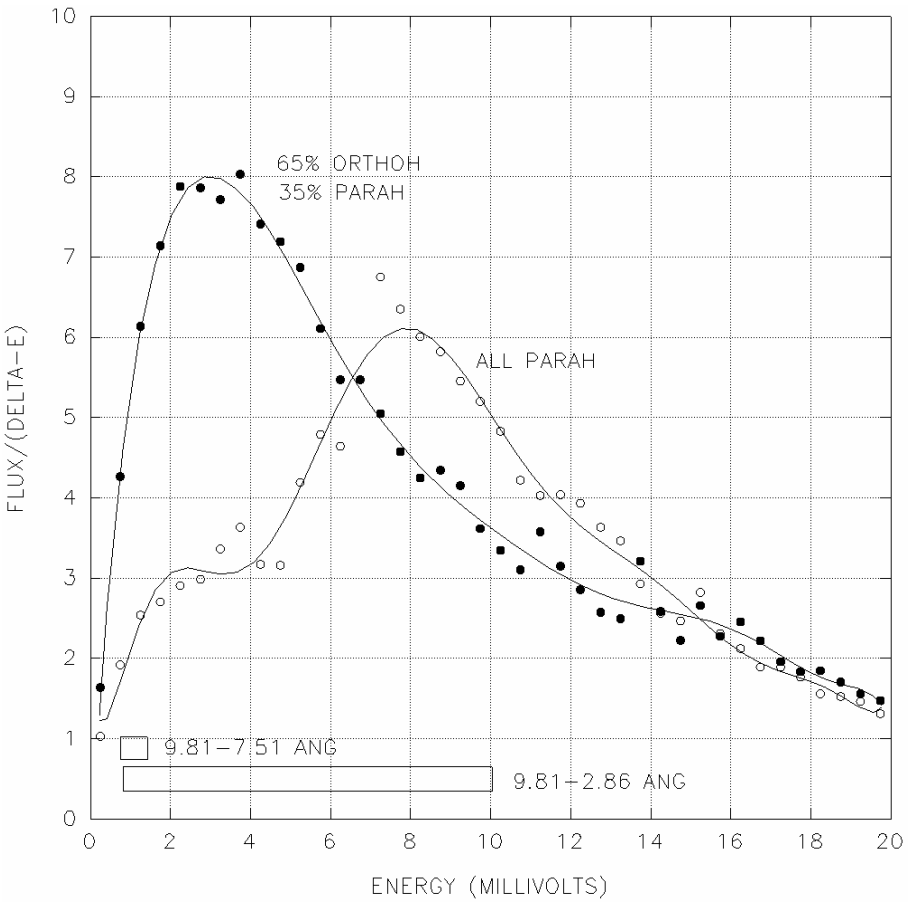

Fig. 8. Ortho hydrogen impact on flux spectrum for the idealized cold source geometry shown in Fig. 7(E). This corresponds to a 14-cm-diam x 2-cm-thick "punctured" spherical shell of LH_2 in a beryllium reflector, with the flux calculated at a point 477.7 cm down a 10-cm-diam beam tube.

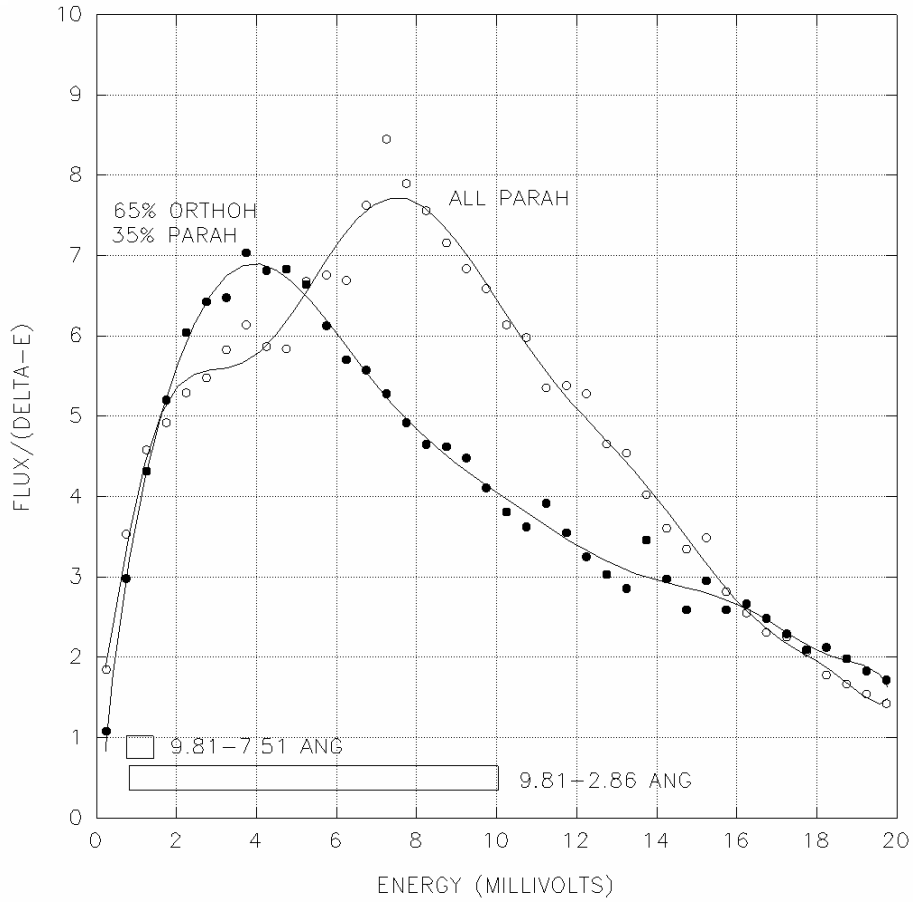

Fig. 9. Ortho hydrogen impact on flux spectrum for the idealized cold source geometry shown in Fig. 7(F). This corresponds to a 10-cm-diam x 2-cm-thick "complete" spherical shell of LH_2 in a beryllium reflector, with the flux calculated at a point 477.7 cm down a 10-cm-diam beam tube.

The results of this evolution study were both interesting and reassuring. They show that MCNP and the existing cross-section datasets could reproduce the results of both the NIST cold source and the HFIR cold source while providing a clear physical understanding of why the sensitivity to the ortho-H content was so markedly different in each case. Specifically, it suggested that, for the proposed HFIR geometry, the cold neutron brightness was relatively insensitive to the ortho/para ratio over the 7- to 10-angstrom wavelength range of interest. This was good news for the development of the HFIR cold source because the relative ortho/para ratio in the high radiation field is not well understood, and could have resulted in a large uncertainty in the optimization of the cold source geometry, if sensitivity to this ratio were high.

More realistic cold source optimization calculations were later performed for the actual cold source geometry (cf. Fig 2) embedded in a full 3-D MCNP model of the HFIR core and reflector (cf. Fig. 1). Here, the thickness of the LH_2 in the nose of the cold source capsule was varied from 2 cm to 8 cm (in increments of 1 cm) by changing the location of the inner ellipsoid forming the inner wall of the capsule. These results are shown in Table 7. In each case, 3-D MCNP calculations were performed with 0%, 20%, 40%, and 60% ortho-H in the LH_2. Note that this optimization for the brightness must necessarily be performed as a simultaneous function of both the thickness of the cold source and the ortho/para ratio in the liquid hydrogen. Because the HFIR cold source is located in a tangential beam tube, its brightness will increase slightly with the thickness of the cold source for the all-para case -- but, at thicknesses greater than about 5 cm, the degradation that might occur if any ortho-H were to develop would become more severe. With increasing thickness, the cryogenic heat load in the liquid hydrogen (and hence the size and cost of the necessary refrigeration unit) would also increase. For these reasons, a hydrogen thickness of 5 cm was judged to be the best design choice for this particular location in this particular reactor system.

4.2. Optimization of Viewing Window Orientation

The cold moderator capsule, when viewed from the beam tube axis, has a circular profile with an outer diameter of 9.843 cm. There is a central reentrant cavity, roughly elliptical in shape, with the inlet and outlet tubes displaced outward along the short axis of the cavity and located near the outer circular boundary. An imaginary “viewing rectangle” inscribed in this central cavity would measure 6.728 x 3.81 cm. The question of the best orientation of this rectangle relative to rotation about the beam tube axis was evaluated to determine the preferred orientation of the inlet and outlet hydrogen lines (i.e., lines must fit outside of the inscribed viewing rectangle). A horizontal beam orientation means that the long axis of the central elliptical cavity is horizontal, and that the inlet and outlet tubes are aligned in the vertical direction. A rotation through 90 degrees about the beam tube axis takes the horizontal orientation into the vertical orientation.

If the cold source were to be operated with the hydrogen moderator in the liquid phase at a pressure of 4 bars and a density of 0.0762 g/cc, the placement of the horizontal outlet tube above the horizontal inlet tube would be preferred from a mechanical design perspective because of the phase change issue. However, if nominal operation were restricted to a higher working pressure of 15 bars, thus putting the hydrogen in a supercritical (almost gaseous) regime having essentially the same mass density, the orientation of the coolant tubes is less important with respect to the mechanical design of the cold source. [In the final design, this higher pressure was selected.]

From the neutron scattering point of view, the orientation question hinges on the issue of source brightness uniformity. If the source were uniformly bright over the full circular area (9.843 cm diam), the orientation would be immaterial, and a horizontal beam orientation would be chosen because the mechanical support of the cold source capsule is somewhat easier in this orientation. However, if the brightness in the central elliptical cavity were significantly greater than that of the remainder of the source area, a vertical beam orientation would be

Table 7. Relative brightness as a function of the HFIR cold source thickness (t), % ortho-H (x), and wavelength (w), where the relative brightness is defined as RB(t,x,w) = B(t,x,w) / B (5,0,w)

Thk.	Wavelength	0% ortho-H		20% ortho-H		40% ortho-H		60% ortho-H	
cm	(angstroms)	Ratio	fsd	Ratio	fsd	Ratio	fsd	Ratio	fsd
2	11.93 - 15.86	.733161	.0350	.664356	.0376	.669772	.0365	.666982	.0371
2	9.81 - 11.93	.711406	.0301	.736855	.0306	.723163	.0318	.747382	.0319
2	7.51 - 9.81	.738706	.0201	.765082	.0210	.832199	.0215	.839231	.0214
2	5.02 - 7.51	.741232	.0164	.767244	.0173	.826831	.0173	.870002	.0173
2	2.86 - 5.02	.802677	.0098	.729118	.0104	.729964	.0106	.717815	.0109
2	0.89 - 2.86	1.226262	.0094	1.150740	.0097	1.122351	.0097	1.119701	.0099
3	11.93 - 15.86	.834215	.0330	.746864	.0358	.687202	.0362	.706856	.0364
3	9.81 - 11.93	.823421	.0285	.794803	.0297	.770827	.0292	.804652	.0295
3	7.51 - 9.81	.844228	.0190	.864964	.0201	.897818	.0205	.910348	.0206
3	5.02 - 7.51	.848048	.0159	.872341	.0170	.925879	.0168	.957036	.0172
3	2.86 - 5.02	.889776	.0097	.801436	.0101	.780121	.0104	.778005	.0106
3	0.89 - 2.86	1.125469	.0094	1.036138	.0097	.997423	.0099	.990601	.0100
4	11.93 - 15.86	.954127	.0332	.759817	.0354	.747595	.0369	.706975	.0372
4	9.81 - 11.93	.916091	.0271	.792971	.0288	.820027	.0290	.800483	.0298
4	7.51 - 9.81	.973518	.0231	.891077	.0204	.924244	.0206	.895996	.0206
4	5.02 - 7.51	.923203	.0157	.924063	.0164	.946734	.0167	.947135	.0175
4	2.86 - 5.02	.946346	.0095	.833284	.0106	.793304	.0103	.778152	.0113
4	0.89 - 2.86	1.043996	.0093	.942607	.0097	.910567	.0100	.905039	.0100
5	11.93 - 15.86	1.000000	.0263	.763473	.0356	.689415	.0356	.673190	.0381
5	9.81 - 11.93	1.000000	.0225	.810306	.0284	.785338	.0312	.748330	.0304
5	7.51 - 9.81	1.000000	.0153	.912784	.0197	.893252	.0226	.870760	.0209
5	5.02 - 7.51	1.000000	.0175	.930151	.0164	.942986	.0169	.936937	.0169
5	2.86 - 5.02	1.000000	.0081	.833778	.0099	.777148	.0102	.747236	.0106
5	0.89 - 2.86	1.000000	.0081	.877714	.0097	.842992	.0101	.830806	.0104
6	11.93 - 15.86	1.007078	.0307	.692068	.0348	.674706	.0368	.643600	.0388
6	9.81 - 11.93	1.044769	.0271	.826886	.0294	.765390	.0301	.733890	.0307
6	7.51 - 9.81	1.049487	.0173	.910443	.0197	.868159	.0209	.854350	.0208
6	5.02 - 7.51	1.022406	.0154	.935418	.0166	.934765	.0168	.887303	.0170
6	2.86 - 5.02	1.036021	.0094	.824064	.0100	.772904	.0104	.720696	.0107
6	0.89 - 2.86	.960836	.0093	.824265	.0099	.789626	.0102	.780755	.0103
7	11.93 - 15.86	1.061260	.0294	.686020	.0355	.671362	.0383	.605989	.0372
7	9.81 - 11.93	1.090486	.0257	.751833	.0294	.751513	.0307	.710125	.0311
7	7.51 - 9.81	1.109605	.0171	.852959	.0199	.861102	.0204	.804525	.0211
7	5.02 - 7.51	1.065461	.0153	.900661	.0164	.895562	.0168	.862492	.0173
7	2.86 - 5.02	1.064559	.0092	.802822	.0099	.732518	.0104	.695280	.0107
7	0.89 - 2.86	.925900	.0093	.767902	.0100	.744808	.0103	.750299	.0106
8	11.93 - 15.86	1.118796	.0287	.707495	.0361	.608489	.0368	.614156	.0394
8	9.81 - 11.93	1.138643	.0247	.765851	.0306	.739608	.0398	.661911	.0312
8	7.51 - 9.81	1.112229	.0171	.842880	.0200	.791503	.0207	.767997	.0211
8	5.02 - 7.51	1.093826	.0151	.882281	.0164	.843395	.0170	.824821	.0175
8	2.86 - 5.02	1.073700	.0091	.783783	.0100	.704297	.0105	.660958	.0108
8	0.89 - 2.86	.897906	.0093	.734276	.0101	.700598	.0103	.706843	.0107

preferred. Moreover, for experiments employing a crystal monochromator diffracting in the horizontal plane, the vertical orientation of the beam would give better resolution for equal signal strengths due to the smaller horizontal divergence of the beam incident on the monochromator.

To resolve this question, Monte Carlo calculations were performed to determine the average brightness over the full circular area (76.09 cm^2) and over the inscribed rectangle in the central elliptical cavity (25.63 cm^2). These calculations were made by placing a thin but infinitely black masking shield midway down the beam tube. The results are summarized in Table 8, which gives the ratio of the average brightness over the inscribed rectangle to that of the full circle.

Somewhat surprisingly, the two brightnesses were nearly equal for all wavelengths of interest, indicating a nearly uniform brightness over the full circular area. The gradual increase in this ratio as the wavelength increases indicates a slightly cooler spectrum for the inscribed rectangle compared to the full circle. While this study gives no compelling reason to favor a particular orientation from the neutron scattering point of view, the ORNL scattering group initially favored a vertical orientation. [Since the completion of the conceptual design described here, the inner cavity has been widened in both directions, and the final design (dated August 1999) now features an inner cavity that is elongated in the vertical direction, with the coolant tubes lying in a common horizontal plane.]

Table 8. Brightness Ratio (inscribed rectangle / full circle)

Wavelength (angstroms)	Brightness ratio
2.86 to 5.02	0.936 ± 0.009
5.02 to 7.51	0.998 ± 0.016
7.51 to 9.81	1.046 ± 0.020
9.81 to 11.93	1.048 ± 0.030
11.93 to 15.86	1.086 ± 0.036
15.86 to 28.60	1.178 ± 0.047

4.3. Effect of the Cold Source (in HB-4) on Experiments That Use HB-1

The HB-1 and HB-4 beam tubes are oriented 180 degrees from each other. The two tubes are separated by a small beryllium block. There was concern within the user community that the presence of the cold source in the HB-4 beam tube might cause some undesirable perturbations for the user station located at the end of the HB-1 beam tube. While it is true that the presence of the liquid hydrogen in the cold source will modify the spectrum of the neutrons in and around the HB-4 beam tube, it was noted that very little beryllium and water at normal reflector temperature is required to return the spectrum to that normally expected in the reflector. Moreover, because the neutrons immediately surrounding the cold source are not expected to contribute to the source at HB-1, it was believed that the presence of the cold source should have very little (if any) effect on flux levels at the end of the HB-1 beam tube. However, an analysis was performed to verify this belief. At first glance (see Table 9), some spectrum changes are visible. However, upon

closer evaluation one finds that, for all energy groups, a ratio of 1.00 is within the statistically derived uncertainty factor. Based on these findings, the fluxes at the instrumented end of HB-1 will not be significantly affected by the presence or absence of LH_2 in the cold source capsule located in HB-4.

Table 9. Comparison of relative fluxes[a] in HB-1, with and without the cold source in HB-4.

Energy range (eV)	With LH_2 cold source	Without LH_2 cold source	Ratio
1×10^5 - 2×10^6	0.050 ± 0.002	0.052 ± 0.002	0.96
1×10^2 - 1×10^5	0.111 ± 0.003	0.107 ± 0.003	1.04
0.625 - 100.0	0.099 ± 0.003	0.097 ± 0.003	1.02
0.104 - 0.625	0.115 ± 0.003	0.114 ± 0.003	1.01
0.010 - 0.104	0.597 ± 0.010	0.596 ± 0.009	1.00
0.00325 - 0.01	0.031 ± 0.001	0.029 ± 0.001	1.07
0.00145 - 0.00325	0.0034 ± 0.0002	0.0034 ± 0.0002	1.00
0.00085 - 0.00145	0.0006 ± 0.00007	0.0005 ± 0.00006	1.20
<0.00085	0.00020 ± 0.00003	0.00019 ± 0.00003	1.05
Total	1.01 ± 0.01	1.00 ± 0.01	1.01

[a] All fluxes are normalized relative to the total neutron flux in HB-1, without the LH_2 cold source in HB-4. The ratio represents the expected nominal change in the HB-1 neutron flux when the LH_2 cold source is added to the system.

4.4. Extent of Accelerated Silicon Production in the Beam Tube(s)

With a much more intense source of cold neutrons now located in the HB-4 beam tube, there was some concern over the extent to which this might accelerate silicon production in the aluminum beam tube. This process of transmuting the structural aluminum into silicon occurs when Al-27 absorbs a neutron, becomes Al-28, and very quickly decays via beta emission to become silicon. With many more neutrons present at very low energies, this transmutation process will be accelerated. The question was, "to what extent?" Moreover, since the HB-4 beam tube is a pressure boundary and must have a functional lifetime in excess of seven years, the question had to be addressed.

First, it must be recognized that cold neutrons are readily absorbed and cannot travel very far in most room-temperature materials without being absorbed or upscattered into higher energy levels. The cold neutron flux levels in the HB-4 beam tube will be less than at the tip of the cold source vacuum vessel and/or capsule. At most, the cold neutron flux levels in the hemispherical tip of the HB-4 beam tube will be comparable to those in the hemispherical tip of the aluminum cold source capsule immediately adjacent to the liquid hydrogen in the present neutronic model.

Estimates of the silicon production rate at any position can be readily and reliably estimated from the Al-28 decay-beta heating rates, which were based on the actual steady-state Al-27 absorption rate and an average beta-decay energy of 1.2423 MeV. Using this approach, it was estimated that 0.7% of all the aluminum atoms in the cold source capsule will be converted to silicon every "full power year" (assuming the HFIR is operating at 100 MW, 365.25 full-power days per year). The rate of silicon production in the wall of the HB-4 beam tube close to the cold source vacuum vessel will be less than the 0.7% rate, but not substantially less. This rate of transmutation is believed to be slightly higher than the present transmutation rate and consistent with increases observed for a similar analysis performed for the ANS reactor cold source. The implication of this increase has been factored into component lifetime estimates.

4.5. Impact of the Cold Source on Other HFIR Facilities

The HFIR is a multifunction research reactor that has facilities for isotope production, materials irradiation, and beam experiments. In its current configuration, the HFIR has 12 irradiation positions in the removable beryllium reflector (RBs), 8 irradiation positions in the control rod access plugs (CRs), 22 vertical experiment facilities (VXFs) in the permanent reflector, and the 4 horizontal beam tubes. There are also many irradiation and production positions located in the central hole of the annular fuel element. The proposed cold source represents a change in the configuration of the reflector system, and therefore may have an impact on the neutron fluxes at these facilities. Calculations were performed with and without the cold source to determine its impact on the reactor in terms of the neutron fluxes at these experimental facilities as well as on the core reactivity.

The MCNP calculations for the base case (no cold source) and the perturbed case (with cold source) were performed with 5 million neutron histories. The ratio of the effective multiplication factors (k_{eff} with cold source / k_{eff} without cold source) was determined to be 0.9992. This indicates essentially no reactivity impact on the core.

In addition to the multiplication factors, the neutron fluxes in the RB and VXF positions were also calculated. The results of the calculations for the nearest large RB position (RB-7A), the nearest small RB position (RB-8), and the nearest VXF position (VXF-22) are given in Table 10. The results indicate that the changes in the neutron fluxes in these regions are small and are generally within the MCNP calculational statistics.

5. Conclusion

Extensive physics evaluations have been performed in support of the design for the new cold neutron source to be installed in the HB-4 beam tube of the High Flux Isotope Reactor at ORNL. In the primary wavelength ranges of interest (7.5 to 15.9 angstroms), the brightness of the new HFIR cold source should be comparable to the horizontal cold source at ILL. Calculated gains in brightness (i.e., with vs. without the cold source) are consistent with those seen for other liquid hydrogen cold sources elsewhere. Unlike the cold source at NIST, which has a very different geometry, the brightness of the HFIR cold source in the 7.5 to 9.8 angstrom range is relatively insensitive to the amount of ortho-H that may be present. (This is primarily due to differences in geometry, scattering probabilities, and escape probabilities. NIST has a large thin spherical shell of LH_2 punctured by a large-diameter beam tube, and requires the additional scattering afforded by the ortho-H to maintain the low-energy neutron population, while the HFIR cold source uses a more compact volume of LH_2 which is closer to the optimal thickness of 5.0 cm and has a smaller leakage probability so that the lesser amount of scattering afforded by para-H is still sufficient for near-optimal moderation.) Moreover, 3-D optimization calculations have been performed to study

Table 10. Comparison of neutron fluxes at the RB-7A, RB-8, and VXF-22 experimental locations, with and without the LH_2 cold source in HB-4.

Experimental Location	Energy range (eV)	Neutron fluxes without HB-4 cold source ($s^{-1}cm^{-2}$)	Neutron fluxes with HB-4 cold source ($s^{-1}cm^{-2}$)	Nominal ratio with / without
RB-7A	$>1.83 \times 10^5$	$4.85(\pm0.09)\times10^{14}$	$4.78(\pm0.09)\times10^{14}$	0.99
RB-7A	$101.0 - 1.83 \times 10^5$	$6.85(\pm0.12)\times10^{14}$	$6.90(\pm0.12)\times10^{14}$	1.01
RB-7A	0.414 - 101.0	$4.10(\pm0.07)\times10^{14}$	$4.11(\pm0.07)\times10^{14}$	1.00
RB-7A	<0.414	$1.35(\pm0.02)\times10^{15}$	$1.35(\pm0.02)\times10^{15}$	1.00
RB-8	$>1.83 \times 10^5$	$5.17(\pm0.21)\times10^{14}$	$5.08(\pm0.21)\times10^{14}$	0.98
RB-8	$101.0 - 1.83 \times 10^5$	$6.20(\pm0.26)\times10^{14}$	$6.04(\pm0.25)\times10^{14}$	0.97
RB-8	0.414 - 101.0	$4.32(\pm0.19)\times10^{14}$	$4.06(\pm0.19)\times10^{14}$	0.94
RB-8	<0.414	$1.11(\pm0.03)\times10^{15}$	$1.11(\pm0.03)\times10^{15}$	0.99
VXF-22	$>1.83 \times 10^5$	$4.22(\pm0.27)\times10^{13}$	$4.34(\pm0.28)\times10^{13}$	1.03
VXF-22	$101.0 - 1.83 \times 10^5$	$1.03(\pm0.05)\times10^{14}$	$1.12(\pm0.05)\times10^{14}$	1.09
VXF-22	0.414 - 101.0	$9.92(\pm0.41)\times10^{13}$	$1.11(\pm0.04)\times10^{14}$	1.12
VXF-22	<0.414	$8.39(\pm0.15)\times10^{14}$	$8.50(\pm0.15)\times10^{14}$	1.01

the resulting brightness as a simultaneous function of both the thickness of the cold source and the ortho/para ratio in the liquid hydrogen. Because the HFIR cold source is located in a tangential beam tube, its brightness will increase slightly with the thickness of the cold source for the “all para” case -- but, at thicknesses greater than about 5 cm, the degradation that might occur if any ortho-H were to develop would become more severe. With increasing thickness, the cryogenic heat load in the liquid hydrogen (and hence the size and cost of the necessary refrigeration unit) would also increase. For these reasons, a hydrogen thickness of 5 cm was judged to be the best design choice for this particular location in this particular reactor system. This yields a total cryogenic heat load of about 2.2 kW. Other calculations have shown that the brightness near the inner cavity of the cold source is not significantly different than the brightness near the outer perimeter, thus making moot any physics questions regarding the preferred orientation of the cooling tubes and the resulting inner cavity. [In the final design, the two coolant tubes will lie in a common horizontal plane so that the inner cavity of the cold source and the resulting neutron beam incident on the monochrometer will have a vertical orientation, with minimal divergence and better resolution in the horizontal direction.] Still other physics calculations have shown that about 0.7% of the aluminum atoms forming the cold source capsule and surrounding beam tube will be transmuted into silicon every full-power year. This has, of course, been factored into the various component lifetimes. Lastly, it has been shown that the new LH_2 cold source will have no significant impact on the system reactivity or on the flux levels in any of the other experimental facilities.

REFERENCES

1. R. D. Cheverton and T. M. Sims, "HFIR Core Nuclear Design," ORNL-4621, July 1971.

2. D. L. Selby et al., *High Flux Isotope Reactor Cold Source Preconceptual Design Study Report*, ORNL/TM-13136, Lockheed Martin Energy Systems, Inc., Oak Ridge National Laboratory, December 1995

3. D. L. Selby et al., *High Flux Isotope Reactor Cold Neutron Source Reference Design Concept*, ORNL/TM-13498, Lockheed Martin Energy Systems, Inc., Oak Ridge National Laboratory, May 1998

4. P. Ageron, "Neutronic Design of the ILL Cold Sources: An Historical Perspective," *Proceedings of the International Workshop on Cold Neutron Sources*, 1-18, LA-12146-C, cosponsored by Los Alamos National Laboratory's Manuel Lujan Jr. Neutron Scattering Center (LANSCE) and the Oak Ridge National Laboratory Advanced Neutron Source (ANS) Project, August 1991.

5. J. F. Breismeister, *MCNP – A General Monte Carlo N-Particle Transport Code, Version 4B*, LA-12625-M, Los Alamos National Laboratory, Los Alamos, New Mexico, March 1997.

6. O. W. Hermann and R. M. Westfall, "ORIGEN-S: SCALE System Module to Calculate Fuel Depletion, Actinide Transmutation, Fission Product Buildup and Decay, and Associated Radiation Source Terms," as contained in Vol. 2, Sect. F7 of *SCALE: A Modular Code System for Performing Standardized Computer Analyses for Licensing Evaluation*, ORNL/NUREG/CSD-2/V2/R5, Oak Ridge National Laboratory, March 1995.

7. R. E. MacFarlane, *New Thermal Neutron Scattering Files for ENDF/V-VI Release 2*, LA-12639-MS, Los Alamos National Laboratory, Los Alamos, New Mexico, March 1994.

8. R. T. Primm, III, *Reactor Physics Input to the Safety Analysis Report for the High Flux Isotope Reactor*, ORNL/TM-11956, Lockheed Martin Energy Systems, Inc., Oak Ridge National Laboratory, March 1992.

9. J. A. Bucholz, *Initial Global 2-D Shielding Analysis For the Advanced Neutron Source Core and Reflector*, ORNL/TM-12672, Lockheed Martin Energy Systems, Inc., Oak Ridge National Laboratory, August 1995.

10. Y. Farawila, Y. Gohar, and C. Maynard, *KAOS/LIB-V: A Library of Nuclear Response Functions Generated by the KAOS-V Code from ENDF/B-V and Other Data Files*, ANL/FPP/TM-241, Argonne National Lab, April 1991.

11. J. M. Carpenter, "Cold Moderators for Pulsed Neutron Sources," *Proceedings of the International Workshop on Cold Neutron Sources*, 131-154, LA-12146-C, cosponsored by Los Alamos National Laboratory's Manuel Lujan Jr. Neutron Scattering Center (LANSCE) and the Oak Ridge National Laboratory Advanced Neutron Source (ANS) Project, Aug 1991.

12. R. E. Williams, J. M. Rowe, and M. Blau, "Benchmark of the Nuclear Heat Deposition in the NIST Liquid Hydrogen Cold Source," Ninth International Symposium on Reactor Dosimetry, Prague, Czech Republic, September 1996.